# Müller cells are living optical fibers in the vertebrate retina

Kristian Franze*, Jens Grosche*†, Serguei N. Skatchkov‡, Stefan Schinkinger§, Christian Foja¶, Detlev Schild‖, Ortrud Uckermann*, Kort Travis§, Andreas Reichenbach*,**, and Jochen Guck§††

*Paul Flechsig Institute of Brain Research, Universität Leipzig, Jahnallee 59, 04109 Leipzig, Germany; †Interdisciplinary Center of Clinical Research, Inselstrasse 22, 04103 Leipzig, Germany; ‡Center for Molecular Biology and Neuroscience, Department of Biochemistry, School of Medicine, Universidad Central de Caribe, Bayamon, Puerto Rico 00960; §Division of Soft Matter Physics, Department of Physics, Universität Leipzig, Linnéstrasse 5, 04103 Leipzig, Germany; ¶Department of Ophthalmology and Eye Clinic, Universität Leipzig, 04103 Leipzig,Germany; ‖Deutsche Forschungsgemeinschaft Molecular Physiology of the Brain Research Center and Department of Neurophysiology and Cellular Biophysics, Universität Göttingen, 37073 Göttingen, Germany; and ††Department of Physics, University of Cambridge, JJ Thomson Avenue, Cambridge CB3 0HE, United Kingdom

Although biological cells are mostly transparent, they are phase objects that differ in shape and refractive index. Any image that is projected through layers of randomly oriented cells will normally be distorted by refraction, reflection, and scattering. Counterintuitively, the retina of the vertebrate eye is inverted with respect to its optical function and light must pass through several tissue layers before reaching the light-detecting photoreceptor cells. Here we report on the specific optical properties of glial cells present in the retina, which might contribute to optimize this apparently unfavorable situation. We investigated intact retinal tissue and individual Müller cells, which are radial glial cells spanning the entire retinal thickness. Müller cells have an extended funnel shape, a higher refractive index than their surrounding tissue, and are oriented along the direction of light propagation. Transmission and reflection confocal microscopy of retinal tissue *in vitro* and *in vivo* showed that these cells provide a low-scattering passage for light from the retinal surface to the photoreceptor cells. Using a modified dual-beam laser trap we could also demonstrate that individual Müller cells act as optical fibers. Furthermore, their parallel array in the retina is reminiscent of fiberoptic plates used for low-distortion image transfer. Thus, Müller cells seem to mediate the image transfer through the vertebrate retina with minimal distortion and low loss. This finding elucidates a fundamental feature of the inverted retina as an optical system and ascribes a new function to glial cells.

fiberoptic plate | glial cells | refractive index | light guides | optical trap

**B**iological cells and tissues are usually fairly transparent due to the lack of strong intrinsic chromophores in the visible part of the spectrum and especially in the near-infrared. This transparency is exploited, for example, in multiphoton microscopy, where this low absorption of excitation light leads to relatively large penetration depths. Although such biological objects do not modulate the amplitude of a passing electromagnetic wave, they impart a phase shift due to refractive index variations. This property was recognized by Zernike and used for the contrast enhancement of individual cells in phase-contrast microscopy (1). However, when light passes through multiple layers of cells, as in tissues, images rapidly deteriorate due to scattering events caused by optical and geometrical inhomogeneities with length scales on the order of the wavelength of visible light (2).

Consequently, nature has implemented ingenious solutions in the properties and the arrangement of structures and cell assemblies that light has to pass for normal physiological functioning. The lens body in vertebrate eyes, for instance, consists of elongated fiber cells. These cells do not only display a very regular oval or hexagonal cross-section, a smooth surface, and a regular distribution, they even lose most of their organelles during differentiation, including the cell nucleus (3). In the vertebrate retina, the inner and outer segments of photoreceptor cells are considered natural optical fibers, supported by their highly specialized shape and optical properties (4). Other natural optical fibers occur in deep-sea glass sponges or in the compound eye of insects, whose biomimetic copies have even found their way into technical components (5, 6). What these examples have in common is a relatively regular geometry of the light-guiding structures and, in the case of living cells, a sophisticated specialization for this very function.

Considering these facts, it seems surprising that the retina in the vertebrate eye is inverted and that images projected onto the retina have to pass several layers of randomly oriented and irregularly shaped cells with intrinsic scatterers before they reach the light-detecting photoreceptor cells (7, 8). This situation seems to be "equivalent to placing a thin diffusing screen directly over the film in your camera" (9). However, this "screen" contains a regular pattern of cells, which are arranged in parallel to each other and span the entire thickness of the retina ($\approx$150 $\mu$m). These cells, Müller cells, are radial glial cells in the inner vertebrate retina, which have a cylindrical, fiber-like shape (their original name was "radial fibers of Müller") (10). They fulfill a wide range of physiological functions to support the functioning and survival of retinal neurons (11). For this purpose Müller cells are, unlike the natural optical fibers mentioned above, endowed with many complex side branches, which ensheath neuronal compartments, such as synapses (12). On the other hand, they putatively occupy a strategic position in the path of light through the retina from the vitreous, where light enters the tissue, to the outer limiting membrane, where the inner segments of the photoreceptor cells receive the incident light. Therefore, it is intriguing to investigate whether they could play a role in the transfer of light through the inner retina.

## Results

As a first step to characterize the retina as a phase object, we investigated freshly dissected guinea pig eyes by using modified transmission microscopy (Fig. 1 *a* and *b*). Physiological illumination was simulated by insertion of an optical fiber as a light source into the eye cup. Images were obtained by scanning a plane close to the outer plexiform layer, corresponding to the

© 2007 by The National Academy of Sciences of the USA

BIOPHYSICS
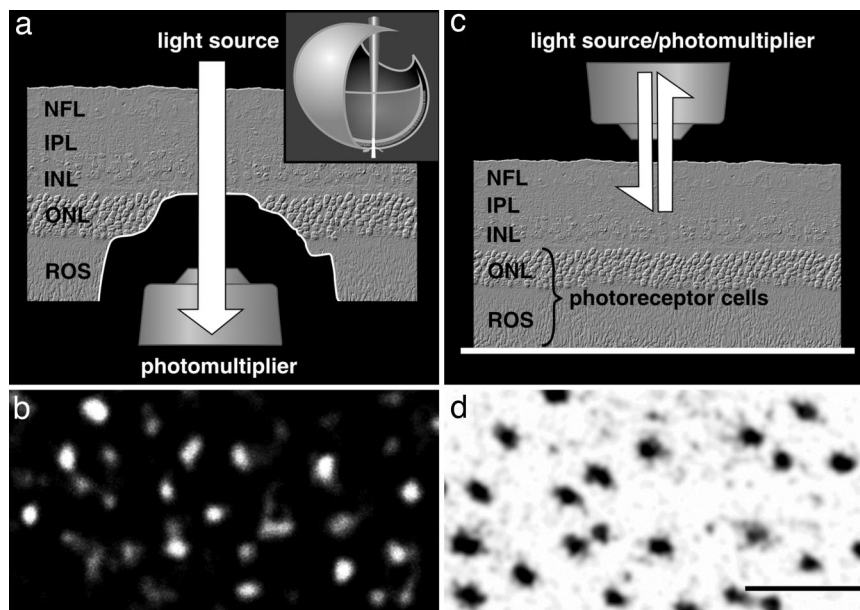
**Fig. 1.** Light transmission and reflection in the inner retina. (*a*) Experimental design to study light transmission through the inner retina. (*Inset*) Light emanating from a multimode optical fiber inserted into a freshly dissected eye simulates physiological illumination of the retina. The eye is opened at the posterior side, and all outer structures, including photoreceptor cells, are surgically removed. The laser light ($\lambda$ = 543 nm) that is transmitted through the inner retina (NFL, nerve fiber layer; IPL, inner plexiform layer; INL, inner nuclear layer) is captured at the end of the prephotoreceptor light path with a confocal microscope. ONL, outer nuclear layer; ROS, photoreceptor outer segments. (*b*) Confocal transmission image of a living unstained retina. The brighter the signal, the more light is relayed to the corresponding area of the tissue. (*c*) Light reflection in the inner retina. Laser light is delivered via the microscope objective of an upright confocal microscope, and light scattered back from inner retinal layers is detected. (*d*) Confocal reflection image at the level of the IPL. The brighter the signal, the more light is reflected by the corresponding area. (Scale bar, 10 $\mu$m; also applies to *b*.)

end of the "prephotoreceptor" light path. Remarkably, these images showed a high degree of inhomogeneity, revealing an almost regular pattern of bright spots alternating with areas of lower transmittance (Fig. 1*b*). This pattern showed that some retinal structures relayed light better than others.

Interpreting the dark areas in Fig. 1*b* as areas of higher scattering, laser scanning measurements in reflection mode (Fig. 1 *c* and *d*) should approximately yield the negative of the above image. Following this hypothesis, we took series of 50–60 consecutive optical sections from flat-mounted retinae. The vitreous body did not reflect any light, consistent with its lack of phase variations. In contrast, the almost uniform reflectance throughout much of the retinal thickness was interrupted by a fairly regular pattern of dark, less reflective spots (Fig. 1*d*). The spots had diameters of 2–3 $\mu$m and were spaced $\approx$5–6 $\mu$m apart, corresponding well to diameter and spacing of the bright spots in Fig. 1*b* [see also supporting information (SI) Fig. 5]. The same reflection patterns were also observed in retinae of rabbits (data not shown) and humans (SI Fig. 6). To show that the observed phenomenon is relevant in physiological conditions, these experiments were successfully repeated with retinae of living guinea pigs *in situ* (SI Fig. 7*d*).

Importantly, reconstruction along the *z* axis (Fig. 2*a* and SI Figs. 6 and 7) showed that the dark spots were contiguous in adjacent horizontal sections and formed tubes that corresponded to distinct optical pathways. At the innermost retinal layer, closest to the vitreous body, these tubes widened to funnel-like structures, which together formed a 15-$\mu$m-thick continuous low-reflecting zone only interrupted by axon bundles (Fig. 2*a*).

The amount of back-scattering from the retina has previously been measured to be 1–5% of the incident light (7, 8). Because biological tissues are typically strongly forward-scattering (13), the total amount of scattering in the retina is most likely at least a factor of 2 larger. The distribution of this scattering within the retina is shown in Fig. 2*a*. Significant back-scattering occurred in all retinal layers proximal to the photoreceptors with the exception of the tubes. The main locations of light scattering are both plexiform layers and the axon bundles (Fig. 2*b*), which contain numerous light-scattering objects with sizes on the order of the wavelength of visible light (14–16) such as "synaptosomes," bundles of neurofilaments, and neurotubules. In combination, our transmission and reflection measurements demonstrate the presence of tubular structures in the retina that transmit significantly more light than their surrounding tissue.

The observed spatial pattern of these tubes corresponded well to the spacing and diameters of the columnar Müller cells (Fig. 2*b*) (17, 18). Furthermore, the funnel-like structures observed in reflection-mode were reminiscent of the densely packed cobblestone pattern of the Müller cell endfeet at the inner retinal surface (19). Indeed, the tubular structures could be unambiguously identified as Müller cells. They were capable of selective uptake of vital dyes (Fig. 2 *b–g*) (20, 21) and could be counterstained with an antibody directed against vimentin (Fig. 2 *f* and *g*). In the retina, vimentin is a protein specific to Müller cells (17, 22). Hence, it is the Müller cells that provide a passage for light through the retina to the photoreceptor cells. These data, together with their cylindrical geometry, suggested a mechanism of light transport similar to optical fibers.

In classical optical fibers, light is confined in the transverse direction by an elevated refractive index of the core compared with its cladding. Thus, we analyzed the refractive indices of enzymatically dissociated vital retinal cells by using quantitative phase microscopy (Fig. 3) (23, 24). The somata of various retinal neurons (ganglion, amacrine, and bipolar cells) displayed similar refractive indices ($n = 1.358 \pm 0.005$; mean $\pm$ SD) (Fig. 3*a*) close to earlier estimates for the total retina (25–27). In contrast, the mean refractive index of Müller cell stalks was significantly higher ($n = 1.380 \pm 0.021$) (Fig. 3*a*). Toward the so-called endfoot, the funnel-shaped termination of the Müller cell facing the vitreous body with $n = 1.335$ (26), the refractive index

Franze et al.
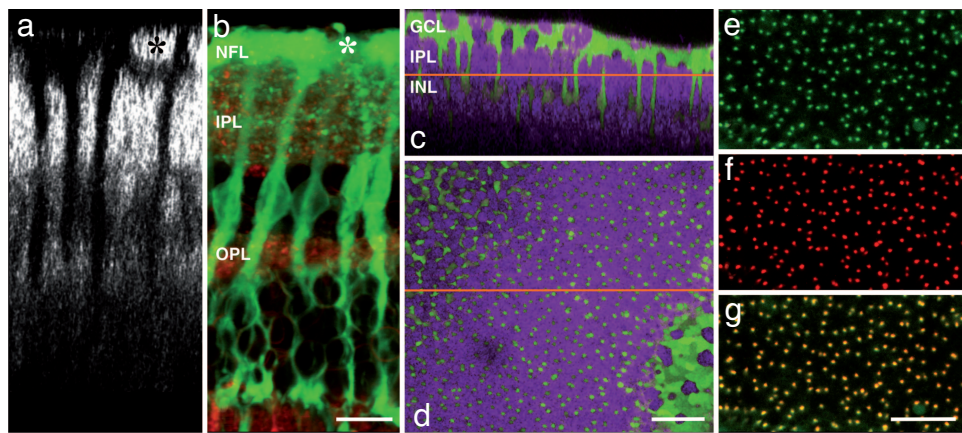
**Fig. 2.** Structures of low reflection are Müller cells. (*a*) Z-line reconstruction of reflection images of a living retina. The main scattering elements (bright) are the axon bundles and both plexiform layers. Low-reflecting tubular structures span the entire retina. (*b*) Living retinal slice preparation, visualizing Müller cells with the vital dye CellTracker orange (green) and synaptic elements in both plexiform layers (IPL and OPL) with the activity-dependent dye FM1–43 (red) (20). The levels of the inner and outer plexiform layers (IPL and OPL, respectively) and nerve fiber layer (NFL) are the same as in *a*. The asterisks indicate axon bundles in the NFL. (*c* and *d*) Overlay of light detected in reflection mode (purple) and the green fluorescence of the vital dye CellTracker green. (*c*) Z-line reconstruction of a confocal image stack. (*d*) Oblique optical section at the level of the red horizontal line in *c*. The dye-filled irregularly shaped Müller cell somata of the inner nuclear layer (INL) are visible in the left upper part. The central area shows Müller cell cross-sections in the IPL. In the lower right part, the Müller cell endfeet are visible, which enclose the ganglion cell somata in the ganglion cell layer (GCL). The lack of merging of the two colors, which would result in white areas, demonstrates that the dye filled exclusively those structures that showed low light reflection. (*e–g*) Confocal image at the IPL of a retinal whole mount fixed in 4% paraformaldehyde after exposure to the green vital dye and immunocytochemical labeling of vimentin (red), which in the retina is specific to Müller cells (17, 22). (*e*) Fluorescence of the vital dye. (*f*) Vimentin immunofluorescence. (*g*) Overlay of *e* and *f*. Colocalization of the red and green dyes results in yellow labeling. The observed complete colocalization means that the vital dye-filled and the immunoreactive cells are identical and thus identifies the low-reflecting tubular structures as Müller cells. [Scale bars: *b*, 10 μm (also applies to *a*); *c–g*, 25 μm.]
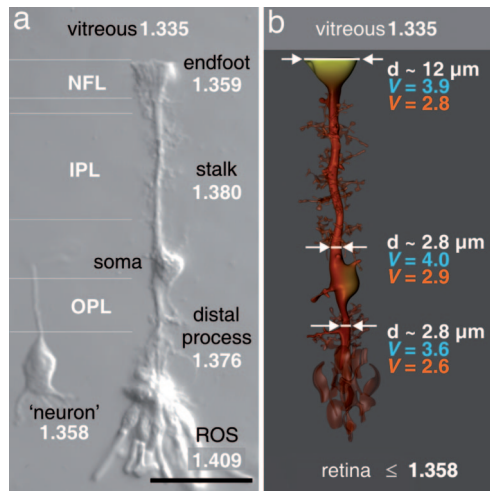
decreased to $n = 1.359 \pm 0.003$. Such a local decrease of the refractive index could serve to minimize reflection at the interface between vitreous and retina. Similar results were consistently found in Müller cells from four different vertebrate species (SI Table 1).

Both the observed differences between the refractive indices of Müller cells and their surroundings as well as the fiber-like cell



**Fig. 3.** Müller cell shape, refractive properties, and light-guiding capability. (*a*) Nomarski differential interference contrast microscopy image of a dissociated guinea pig Müller cell with several adherent photoreceptor cells, including their outer segments (ROS) and a dissociated retinal neuron (bipolar cell) to the left. The refractive indices of the different cell sections are given. (*b*) Schematic illustration of a Müller cell *in situ*. The lighter the coloring of the Müller cell, the lower the refractive index. Typical diameters and the calculated V parameters for 700 nm (red) and 500 nm (blue) are indicated at the endfoot, the inner process, and the outer process. Although diameters and refractive indices change along the cell, its light-guiding capability remains fairly constant. (Scale bar, 25 μm.)
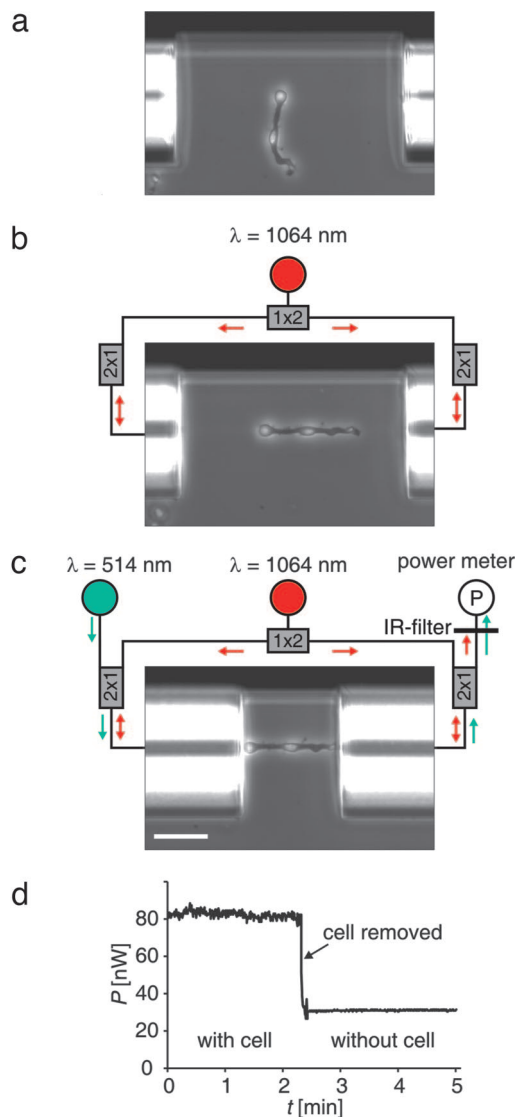
shape are reminiscent of the basic requirements of optical fibers. However, Müller cells display a complex morphology (Fig. 3), and their radius is comparable to the wavelength of light so that the typical total-internal-reflection model of light guidance is not applicable. In a waveguide, light propagates in certain patterns, or modes, determined by boundary conditions following electromagnetic theory (28). Light guidance only occurs if propagating modes exist. The key parameter most widely used in optical engineering to evaluate the presence of propagating modes is the waveguide characteristic frequency, or V parameter,

$$V = \frac{\pi d}{\lambda} \sqrt{n_1^2 - n_2^2},$$

where $\lambda$ is the free-space wavelength of the visible light, $d$ is the diameter of the waveguide, and $n_1$ and $n_2$ are the refractive indices of the waveguide and the surrounding material, respectively (28, 29). For a conservative estimate, it is sufficient to calculate V at the longest visible wavelength (700 nm) and the smallest diameter, which occurs at the inner process ($d \approx 2.8$ μm) (21). The largest possible value for the extracellular refractive index is that of the adjacent neurons with $n_2 = 1.358$. The calculated $V = 2.6–2.9$ for the different parts along the Müller cell (Fig. 3*b*) is sufficiently high to allow low-loss propagation of a few modes in the structure even at 700 nm (28). At a wavelength of 500 nm, the V parameter increases to $V = 3.6–4.0$. Although the refractive index and diameter of the Müller cells both change along their length, the V parameter and, thus, the light-guiding capability stay nearly constant (Fig. 3*b*). In contrast to the smooth cylindrical shape of artificial or other biological optical fibers (6, 30, 31), each cell possesses complex side-branching processes important to its interactions with neurons (12). Their inclusion through an "effective" refractive index gradient actually increases the V parameter of the Müller cell (32). Consequently, despite their complex morphology, Müller cells could thus function as waveguides for visible light.

**Fig. 4.** Demonstration of light guidance by individual Müller cells measured in a modified dual-beam laser trap. (*a*) A cell is floating freely between the ends of two optical fibers, which are aligned against a backstop visible at top. (*b*) The Müller cell is trapped, aligned, and stretched out by two counter-propagating near-infrared laser beams diverging from the optical fibers (42). (*c*) The fibers are brought in contact with the cell. Visible light ($\lambda = 514$ nm) emerges from the left (input) fiber and is collected and guided by the cell to the right (output) fiber. The fraction of visible light reentering the core of the output fiber is measured by a power meter, and the near-infrared light is blocked by an appropriate short-pass filter. (Scale bar, 50 $\mu$m.) (*d*) Typical time course of the power of visible light measured. When the cell is removed from the trap, it no longer prevents the light from diverging, and the measured power drops considerably. The ratio $\eta = P_{with\_cell}/P_{without\_cell}$ defines the relative guiding efficiency.

To test this hypothesis, we investigated light propagation through individual, enzymatically dissociated living Müller cells by using a fiberoptical dual-beam laser trap (Fig. 4) (33–35). The optically induced forces in the trap allowed the gentle capture of individual cells from suspension (Fig. 4*b*). The forces also aligned the cells along the optical axis without any mechanical contact (Fig. 4 *b* and *c*). In addition to the infrared trapping laser beams, visible light was coupled into one of the fibers (input fiber), and the light power coupled back into the opposing (output) fiber was measured (Fig. 4 *c* and *d*). Because the light reentering the output fiber depends on the distance from the input fiber and on the optical properties of the

trapped object, this setup could be used to directly test the axial light transmission through individual cells.

With a Müller cell present in the trap surrounded by media with refractive indices up to 1.36 (to mimic the surrounding in the retina), light transmission into the output fiber was comparable to the situation where both fibers were in contact, as long as the direction of the light propagation was the same as in the retina. When the Müller cell endfoot was pointing away from the input fiber, significantly less light arrived at the output fiber, most likely because of a less efficient light coupling into the outer cell process.

When the cell was removed, the power measured dropped considerably due to the numerical aperture of the input fiber and the resulting divergence of the laser beam (Fig. 4*d* and SI Figs. 8 and 9). This effect was elucidated when the light path was directly visualized by using a fluorescent vital dye (MitoTracker orange) that was both present in solution and taken up by the cell. The dye was excited by the visible light emanating from the input fiber. Although the laser beam diverged as expected without the cell, the light remained confined to the Müller cell when present in the trap (SI Fig. 8). Both experiments clearly showed that Müller cells capture the visible light, prevent it from diverging, and guide it to their distal end. To further demonstrate the light collection and guidance power of Müller cells, the optical fibers were then intentionally misaligned, so that without a cell almost no light was detected (SI Fig. 9). Even in this case, the Müller cells were still able to capture and guide the light. The relative guiding efficiency, $\eta = P_{with\_cell}/P_{without\_cell}$, increased up to a factor of 9, depending on the angle between the fibers. In combination, our single-cell experiments, the theoretical considerations, and the transmission and reflection measurements strongly suggest that Müller cells are, and function as, optical fibers in the retina, relaying light from the inner surface to the layer of the photoreceptors while bypassing scattering structures present.

## Discussion

These results provide insight into the optical properties of the retina. Most structures in the retina, especially those in the nerve fiber layer and both plexiform layers, are phase objects that necessarily cause light scattering (Fig. 2 and SI Figs. 6 and 7) (14, 36, 37). In contrast, the optical properties and geometry of Müller cells are consistent with those of optical fibers so that they serve as low-scattering conduits for light through the retina. The low scattering is likely due to their peculiar ultrastructure because highly scattering objects, such as mitochondria, are rare, or even absent (38), whereas abundant long thin filaments are oriented along the cell axis (12), thereby setting a dielectric anisotropy as typically seen in photonic crystal fibers. The endfeet of Müller cells cover the entire inner retinal surface and have a low refractive index, allowing a highly efficient entry of light from the vitreous into the Müller cells (Figs. 2 and 3). At the same time, the increasing refractive index together with their funnel shape at nearly constant light-guiding capability (Fig. 3) make them ingeniously designed light collectors (31). These findings along with their general orientation along the light path might well explain the low absolute back-scattering in the retina of only 1–5% reported previously (7, 8).

The collective parallel arrangement of Müller cells in the retina resembles that of optical fibers in fiberoptic plates, which are used to transfer images between spatially separate planes with low loss and low distortion. The structural similarity suggests an analogous function of the Müller cell array *in situ* (SI Fig. 5). The basic fiberoptic plate-like structure is especially characteristic for the retinae of all mammals with the exception of the fovea centralis of humans and higher primates, the region of our retina that is responsible for sharp vision; here, the photoreceptor cells are not obscured by any inner retinal layers at all.

On average, every mammalian Müller cell is coupled to one cone photoreceptor cell (17) (responsible for sharp seeing under daylight conditions, i.e., photopic vision) plus a species-specific

number of rod photoreceptor cells (17) ($\approx$10 in both man and guinea pig), serving low light level (scotopic) vision. Thus, in the case of photopic vision, the parallel array of Müller cells may preserve the initial image resolution by guiding the light directly to their respective cone photoreceptor cell, minimizing image distortion. This array might also serve to improve image contrast by increasing the signal-to-noise ratio (39). In scotopic vision, Müller cells could reduce loss of intensity by minimizing light reflection, particularly at the inner retinal surface. In summary, Müller cells in the retina assume the role of optical fibers and reliably transfer light with low scattering from the retinal surface to the photoreceptor cell layer. At the same time, their funnel-shape leaves >80% of the retinal volume for other cells and the neuronal connectivity (SI Fig. 5) and might thus spatially decouple light transport from neuronal signal processing. The function of glial cells that we describe here explains a fundamental feature of the inverted retina as an optical system.

## Materials and Methods

**Experimental Animals.** Adult guinea pigs of either sex (300–500 g) were used throughout the study if not mentioned otherwise. Animals were deeply anesthetized and killed by an overdose of 2 g/kg urethane administered i.p.

All experiments were carried out in accordance with applicable German laws of animal protection and with the Association for Research in Vision and Ophthalmology Statement for the Use of Animals in Ophthalmic and Vision Research. The protocol of this study was approved by the local ethical committee and adhered to the tenets of the Declaration of Helsinki for experiments involving human tissue.

**Confocal Microscopy.** *Transmission measurements.* Freshly dissected guinea pig eyes were gently opened at opposite areas. Cornea and lens were removed for insertion of a multimode optical fiber. Sclera, choroid, pigment epithelium, and the photoreceptor layers were locally cut away to allow direct optical access to the end of the prephotoreceptor light path. The transmitted light emanating from the optical fiber was captured through the objective ($\times$40, N.A. = 0.75, water immersion) of a confocal microscope (LSM 510 Meta; Zeiss, Oberkochen, Germany).
*Reflection measurements.* Freshly isolated retinal whole-mounts of several species, including man, were placed on a confocal microscope with the inner surface pointing toward the objective ($\times$40, N.A. = 0.75, water immersion) and observed in reflection mode.
*In vivo measurements.* Animals were anesthetized by i.m. application of 50 mg/kg ketamine (Ratiopharm, Ulm, Germany) and 5 mg/kg xylazine (BayerVital, Leverkusen, Germany). Eyes were gently opened *in situ* from rostral, cornea and lens were removed, animals were placed on a confocal microscope (LSM 510 Meta), and the objective ($\times$20, N.A. = 0.5, water immersion) was inserted into the eye. Images were taken in reflection mode.

**Cell Isolation.** Fresh retinal pieces were incubated in $Ca^{2+}$- and $Mg^{2+}$-free PBS containing 0.03–0.1 mg/ml Papain (Boehringer, Mannheim, Germany) for 30 min at 37°C. After washing with PBS containing 200 units/ml DNase I (Sigma, Deisenhofen, Germany), the tissue pieces were gently triturated by a wide-pore pipette to obtain suspensions of isolated cells (40, 41). The supernatant was collected, and PBS was replaced by a physiological salt solution (PSS; 136 mM NaCl/3 mM KCl/1 mM $MgCl_2$/2 mM $CaCl_2$/10 mM Hepes/10 mM D-glucose). The pH of the solution was adjusted to

7.4 by using 1 M Tris. In the case of frog retinae, NaCl was reduced from 136 to 115 to maintain physiological osmolarity.

**Refractometry.** Cells were isolated from retinae of humans (clinical samples), cats, guinea pigs, and frogs (*Rana pipiens*) as described above. The cells were then immersed in a chamber filled with PSS on the stage of an upright phase microscope (MBIN-4; LOMO, St. Petersburg, Russia) and allowed to settle to its bottom. Computer-aided phase microscopy was used to obtain quantitative information about the refractive index distribution within the cells as described in refs. 23 and 24. The use of a water-immersion lens ($\times$40, N.A. = 0.65) yielded a diffraction-limited resolution of 0.4 $\mu$m. Imaging light was filtered by a monochromatic band-pass interference filter ($\lambda$ = 550 $\pm$ 5 nm), polarized, and used to measure differences in refractive index between a cellular compartment and the surrounding PSS solution with known refractive index. Defined samples of other salt solutions as well as rod outer segments were measured as controls. The latter yielded refractive indices of 1.407 $\pm$ 0.009 (frog) and 1.409 $\pm$ 0.025 (guinea pig), which are close to an average 1.41 published previously (31).

**Modified Dual-Beam Laser Trap Experiments.** Individual acutely isolated guinea pig Müller cells were trapped and aligned in a dual-beam laser trap (trapping power 0.1 W in each beam) as previously described (42). The output of a near-infrared fiber laser ($\lambda$ = 1,064 nm; YLD-10-1064; IPG Photonics, Burbach, Germany) was fed into two single-mode fibers (PureMode HI 1060; Corning, Berlin, Germany), which were aligned against a backstop opposing each other on the stage of an inverted microscope (DMIL; Leica, Wetzlar, Germany). An additional laser with a wavelength in the visible range (argon ion laser; $\lambda$ = 514 nm) was coupled into one of the fibers, and a power meter (LM2; Coherent Deutschland, Dieburg, Germany) measured the intensity of visible light that coupled back into the opposing fiber. A short-pass filter was used to exclude the infrared trapping light from detection.

In a series of experiments, the refractive index $n$ of the solution was increased to that of the natural surrounding of Müller cells ($n \approx 1.36$) (25–27) by adding BSA (P-0834; Sigma). The refractive index of that solution was determined with a refractometer (Abbe-Refraktometer AR 4; A. Krüss Optronic, Hamburg, Germany). In a further set of experiments, the fibers' backstop was modified in a way such that the fibers were intentionally misaligned by an angle of $\approx$2–3°.

1. Zernike F (1955) *Science* 121:345–349.
2. Tuchin V (2000) *Tissue Optics* (SPIE Press, Bellingham WA).
3. Maisel H (1985) *The Ocular Lens: Structure, Function, and Pathology* (Dekker, New York).
4. Snyder AW, Menzel R (1975) *Photoreceptor Optics* (Springer, Berlin).
5. Lee LP, Szema R (2005) *Science* 310:1148–1150.
6. Sundar VC, Yablon AD, Grazul JL, Ilan M, Aizenberg J (2003) *Nature* 424:899–900.
7. Hammer M, Roggan A, Schweitzer D, Muller G (1995) *Phys Med Biol* 40:963–978.
8. Vos JJ, Bouman MA (1964) *J Opt Soc Am* 54:95–100.

9. Goldsmith TH (1990) *Q Rev Biol* 65:285–287.
10. Schultze M (1866) *Zur Anatomie und Physiologie der Retina* (Cohen & Sohn, Bonn, Germany).
11. Bringmann A, Pannicke T, Grosche J, Francke M, Wiedemann P, Skatchkov SN, Osborne NN, Reichenbach A (2006) *Prog Retin Eye Res* 25:397–424.
12. Reichenbach A, Schneider H, Leibnitz L, Reichelt W, Schaaf P, Schumann R (1989) *Anat Embryol* 180:71–79.
13. Cheong WF, Prahl SA, Welch AJ (1990) *IEEE J Quantum Electron* 26:2166–2185.
14. Knighton RW, Jacobson SG, Kemp CM (1989) *Invest Ophthalmol Vis Sci* 30:2392–2402.
15. Boehm G (1940) *Acta Ophthalmol* 18:143–169.
16. de Oliveira Castro G, Martins-Ferreira H, Gardino PF (1985) *Ann Acad Brasil Ciencias* 57:95–103.
17. Reichenbach A, Robinson SR (1995) *Prog Retin Eye Res* 15:139–171.
18. Reichenbach A, Grimm D, Mozhaiskaja N, Distler C (1995) *J Hirnforsch* 36:305–311.
19. Ashton N, Tripathi R (1972) *Exp Eye Res* 14:49–52.
20. Miller RF, Fagerson MH, Staff NP, Wolfe R, Doerr T, Gottesman J, Sikora MA, Schuneman R (2001) *J Comp Neurol* 437:129–155.
21. Uckermann O, Iandiev I, Francke M, Franze K, Grosche J, Wolf S, Kohen L, Wiedemann P, Reichenbach A, Bringmann A (2004) *Glia* 45:59–66.
22. Shaw G, Weber K (1984) *Eur J Cell Biol* 33:95–104.
23. Tychinsky VP, Masalov IN, Pankov VL, Ublinsky DV (1989) *Opt Commun* 74:37–40.
24. Beuthan J, Minet O, Helfmann J, Herrig M, Müller G (1996) *Phys Med Biol* 41:369–382.
25. Chen E (1993) *Ophthalmic Res* 25:65–68.
26. Valentin G (1879) *Arch Physiol* 19:78–105.
27. Nordenson JW (1934) *Acta Ophthalmol (Copenhagen)* 12:171–175.
28. Snyder AW, Love JD (1983) *Optical Waveguide Theory* (Chapman & Hall, New York).
29. Nielsen MD, Mortensen NA, Folkenberg JR, Bjarklev A (2003) *Opt Lett* 28:2309–2311.
30. Tobey FL, Jr, Enoch JM, Scandrett JH (1975) *Invest Ophthalmol* 14:7–23.
31. Winston R (1981) *The Visual Receptor as a Light Collector* (Springer, New York).
32. Sanyal S, Sarkar S (2002) *Opt Eng* 41:2290–2295.
33. Ashkin A (1970) *Phys Rev Lett* 24:156–159.
34. Constable A, Kim J, Mervis J, Zarinetchi F, Prentiss M (1993) *Opt Lett* 18:1867–1869.
35. Guck J, Ananthakrishnan R, Moon TJ, Cunningham CC, Kas J (2000) *Phys Rev Lett* 84:5451–5454.
36. Martins-Ferreira H, de Castro GO (1966) *J Neurophysiol* 29:715–726.
37. Toth CA, Narayan DG, Boppart SA, Hee MR, Fujimoto JG, Birngruber R, Cain CP, DiCarlo CD, Roach WP (1997) *Arch Ophthalmol* 115:1425–1428.
38. Reichenbach A (1989) *J Hirnforsch* 30:513–516.
39. Barten PGJ (1999) *Contrast Sensitivity of the Human Eye and Its Effects on Image Quality* (SPIE, Bellingham, WA).
40. Reichenbach A, Birkenmeyer G (1984) *Z Mikrosk Anat Forsch* 98:789–792.
41. Francke M, Weick M, Pannicke T, Uckermann O, Grosche J, Goczalik I, Milenkovic I, Uhlmann S, Faude F, Wiedemann P, *et al*. (2002) *Invest Ophthalmol Vis Sci* 43:870–881.
42. Lu YB, Franze K, Seifert G, Steinhauser C, Kirchhoff F, Wolburg H, Guck J, Janmey P, Wei EQ, Kas J, Reichenbach A (2006) *Proc Natl Acad Sci USA* 103:17759–17764.